Lab on a Chip

Accepted Manuscript

ROYAL SOCIETY OF CHEMISTRY

www.rsc.org/loc

Lab on a chip RSCPublishing

ARTICLE

FCite this: DOI: 10.1039/x0xx00000x

Generation of stable orthogonal gradients of chemical concentration and substrate stiffness in a microfluidic device

Received 00th January 2015,
Accepted 00th xxxxxxx 2015

DOI: 10.1039/x0xx00000x

www.rsc.org/

S. García[a]‡, R. Sunyer[a]‡, A. Olivares[a,b], J. Noailly[a,b], J. Atencia[c] and X. Trepat[a,d,e]

Cellular responses to chemical cues are at the core of a myriad of fundamental biological processes ranging from development to cancer metastasis. Most of these biological processes are also influenced by mechanical cues such as the stiffness of the extracellular matrix. How biological function is influenced by a synergy between chemical concentration and extracellular matrix stiffness is largely unknown, however, because no current strategy enables the integration of both types of cues in a single experiment. Here we present a robust microfluidic device that generates a stable, linear and diffusive chemical gradient over a biocompatible hydrogel with a well-defined stiffness gradient. Device fabrication relies on patterned PSA (Pressure Sensitive Adhesive) stacks that can be implemented with minimal cost and lab equipment. This technique is suitable for long-term observation of cell migration and the application of traction force microscopy. We validate our device by testing MDCK cell scattering in response to perpendicular gradients of hepatocyte growth factor (HGF) and substrate stiffness.

Introduction

Living cells are continuously exposed to external cues that modify their behavior and ensure an appropriate biological function. Among these cues, soluble chemical factors are known to regulate virtually every biological process including stem cell differentiation[1,2], the guidance of neutrophils towards insult sites[3–5] and the VEGF induction of angiogenesis in healthy and neoplastic tissues[6,7]. Most of these biological processes are also regulated by mechanical cues from the extracellular matrix. Indeed, mechanical cues such as matrix stiffness or intercellular forces have been shown to modify processes like mesenchymal stem cell differentiation[8,9], cell migration[10,11], embryo development[12] and cancer metastasis[13,14]. Recent studies have established cells respond to the combined action of chemical concentration and substrate stiffness[15–20] . This is well illustrated by the Epithelial to Mesenchymal transition (EMT)[21], a key biological switch that alters cell adhesion and motility during normal embryonic development and cancer progression. The EMT is characterized by genetic and epigenetic changes, as well as by alterations in protein expression and posttranscriptional regulation. Ultimately, the EMT leads to a loss in E-cadherin mediated cell-cell adhesion, an increase in cell-matrix adhesion, the acquisition of front/rear polarity, and altered cytoskeleton composition and architecture[22,23]. This behavior can be promoted by growth factors such as hepatocyte growth factor (HGF)[24,25] and it is enhanced by extracellular matrix stiffness[15].

Several experimental strategies have been developed to study the response of cells to chemical cues and their gradients[26–30]. The simplest of such strategies use microneedles[31,32] or heparin-coated microbeads[33,34], which generate an approximate point-diffusion of soluble chemical factors. Although these approaches can trigger strong chemosensing responses by steep diffusive

[a] Institute for Bioengineering of Catalonia (IBEC), Baldiri Reixac 15-21, 08028 Barcelona, Spain. Email: xtrepat@ibecbarcelona.eu. Tel: +34934020265.
[b] Dept. of Information and Communication Technologies (DTIC), Universitat Pompeu Fabra (UPF), 08018 Barcelona.
[c] Dept. of Bioengineering, University of Maryland College-Park, USA.
[d] Facultat de Medicina, Universitat de Barcelona 08036, Barcelona, Spain
[e] Institució Catalana de Recerca i Estudis Avançats, 08010 Barcelona, Spain
‡ These authors contributed equally to this work.

gradients, they provide limited stability of the gradient profile. This limitation has been overcome with microfluidic devices[35–37]. Early designs were based on the controlled mixing of chemical factors flowing inside a network of microchannels[38]. Although these systems enabled long term control of the chemical profile, the convective flow caused a significant shear stress on the cell surface and triggered cell mechano-responses[39]. Recent microfluidic designs overcome this limitation by establishing a purely diffusive chemical gradient using a combination of simple source/sink constructs with flow resistive elements such as hydrogels, membranes with nanopores, or microchannels[40–49].

The effect of substrate stiffness as a mechanical cue is typically studied by using biocompatible substrates with stiffness gradients. This is commonly achieved by varying the crosslink density of a biocompatible polyacrylamide (PAA) hydrogel. Rudimentary stiffness gradients can be obtained by polymerizing two adjacent droplets containing different concentrations of PAA and its crosslinker[10,50]. More precise methods involve the spatial control of PAA photopolymerization either by changing UV exposure with a gray-level mask[51] or by mixing different PAA solutions with a microfluidic device[52]. The limited spatial resolution and experimental flexibility of these methods has recently been improved by covering a PAA mix with an opaque mask, which is displaced at controlled pace to obtain progressive UV exposure[53]. This approach enables to fabricate small hydrogels with controlled stiffness gradients in the range of tens of kPa/mm. While several devices have been developed to control the spatial distribution of soluble chemical factors or substrate stiffness, no current device enables the combination of both. To fill this gap, here we introduce a device that generates a stable, linear and diffusive chemical gradient over a biocompatible PAA hydrogel with a well-defined stiffness gradient. Device fabrication relies on patterned double-sided PSA (Pressure Sensitive Adhesive) stacks that can be implemented with minimal cost and lab equipment. Our device is suitable for long-term monitoring of cell dynamics. Moreover, by inserting reporter fluorescent beads inside the PAA hydrogel, our device can be used to measure cell contractility using traction force microscopy (TFM)[25,54,55]. To validate our device we used the well-characterized scattering assay of Madin Darby Canine Kidney cells (MDCK). MDCK cells are epithelial cells that grow in tight monolayers but undergo consistent cell dispersion as result of HGF induced EMT[15].

Device design and fabrication

Device principle

The device designed in this study comprises two orthogonal gradients, one chemical and one mechanical, so that cells are subjected to independent chemical and mechanical cues depending on their position in the test chamber (Fig. 1A). The chemical gradient is established by diffusion of a soluble

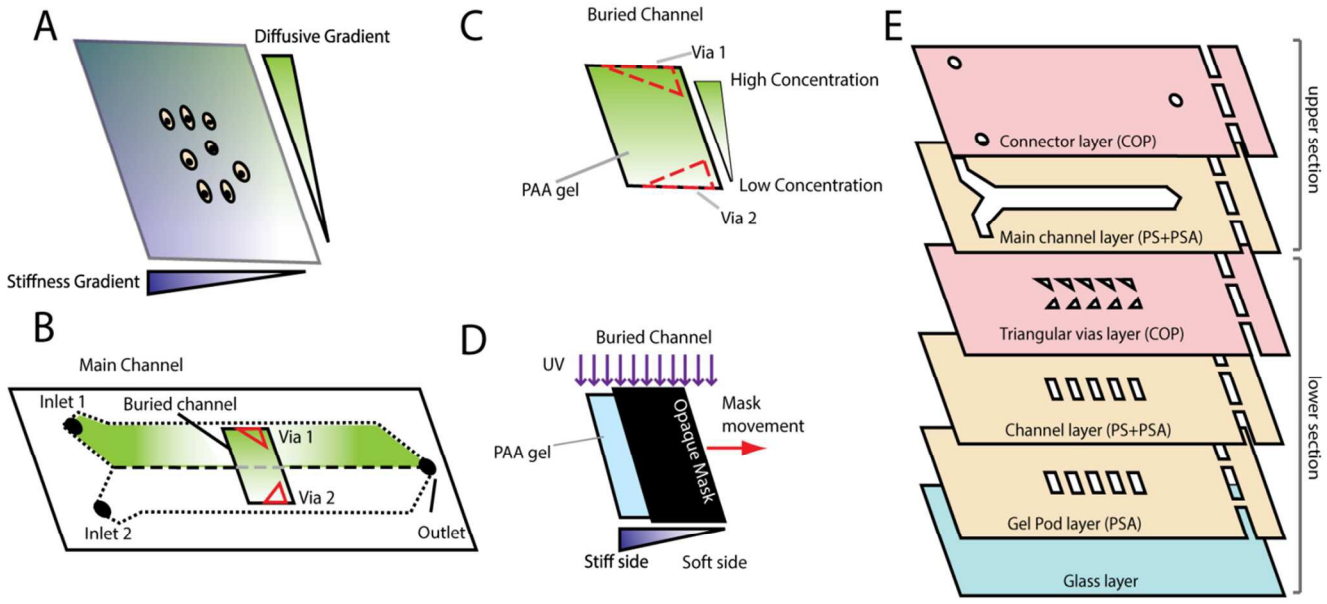

Fig 1. Design of the microfluidic device. (A) The device generates a diffusive chemical gradient perpendicular to a substrate stiffness gradient. (B) The perpendicular chemical and mechanical gradients are generated within a buried channel. The buried channel is placed underneath a Y-shaped main channel and oriented perpendicularly to the direction of the flow inside the main channel. Two triangular vias located at the extremities of each buried channel connect the main channel to the buried channel. (C) When two miscible liquids flow in parallel within the main channel at low Reynolds number, identical pressure is applied to the vias and at both sides of the buried channel, thus establishing a diffusive gradient within it. (D) To generate a stiffness gradient in the biocompatible PAA hydrogel, an acrylamide/bis-acrylamide mix is progressively photo-polymerized by moving an opaque mask at a controlled speed while irradiating with a UV lamp (365 nm). This substrate is functionalized with Collagen I to promote cell adhesion. (E) The microfluidic device comprises a lower and an upper section. The lower section is formed by a glass slide, a PSA layer with rectangular openings (called gel pods) in which PAA-gels are polymerized, a buried channel layer (one PS and one PSA layer), and a vias layer (made of low-auto fluorescence COP laminate). The upper section is an assembly of a Y-shaped 0.5 mm thick main channel stack of PS+PSA, and a final connector layer (made of COP) presenting the inlet/outlet openings.

chemical, while the mechanical gradient is established by varying the stiffness of a PAA hydrogel substrate. The device is based on a Y-shaped main channel with two inlets and one outlet (Fig. 1B). Two different solutions (cell medium and cell medium plus chemical factor) are injected into the device and flowed side by side under laminar regime, with diffusive mixing occurring at the interface between both. Two triangular openings (termed vias) connect the main channel to an underlying "buried" channel (Fig. 1B, red triangles). We chose a triangular shape because it favors symmetry of the flow patterns in the buried channel but circular and rectangular vias are also effective (see Supplementary Note 1). The vias are located at the same cross section of the main channel, and away from the diffusive interface; thus, each via is exposed to full concentration of each solution, and both are subject to equal pressure. This results in the automatic generation of a diffusive chemical gradient within the buried channel (Fig. 1C). The buried channel contains a biocompatible PAA hydrogel with a stiffness gradient perpendicular to the chemical gradient. The stiffness gradient is obtained by irradiating an acrylamide/bis-acrylamide mix initially protected by an opaque mask (Fig. 1D). By moving the mask at constant speed, we achieve a non-uniform illumination pattern that creates a stiffness gradient. The final device combines different layers of PSA, polystyrene (PS), and cyclic olefin polymer (COP) (Fig. 1E). While PSA and PS layers provide robust sealing and optimal adhesive intercalation, COP layers ensure low autofluorescence and optimal compatibility with fluorescence microscopy.

Device assembly

The fabrication process was adapted from the method described by Atencia and co-workers[56] (Fig. 1 and Supplementary Fig. S1). Briefly, a microfluidic device is built by stacking adhesive and plastic laminates patterned with a desktop digital craft cutter (Cameo Silhouette). The design consists of two functionally distinct channels: the main channel and the buried channel. In the main channel, two solutions (Fig. 1B) flow side by side in the laminar regime. In the buried channel (underlying orthogonal test chamber) solutes from the source solution diffuse passively through small openings (vias, Fig. 1B and Fig. 1C). An arbitrary number of buried channels can be implemented in parallel for each main channel (in our case, 5 buried channels).

To facilitate assembly, the device is subdivided into a lower and an upper section. The lower section bears the gel, the buried channels, and the vias. It is assembled as follows. A first layer of PSA (Adhesive Research) containing 5 rectangular holes (gel pods, 4.5×2.5 mm) is adhered onto a silanized glass slide. The PAA hydrogel is then polymerized with a stiffness gradient (See the "PAA hydrogel polymerization" section). The next step is the fabrication of the layer containing the buried channel. This layer is formed by stacking a layer of PS and a layer of PSA for a total height of 220 µm. It contains 5 rectangular holes which are slightly smaller (4×2 mm) than gel pods to adapt to the actual gel size. The vias are cut in a separate layer made of low auto-fluorescence COP (Zeon Chemicals) with a thickness of 180 µm.

We use triangular shapes in order to reduce the convective flow entering the main channel. Once the buried channel layer and the vias layers are stacked on top of the gel pod layer, the lower section of the device is ready for cell seeding (See "Cell loading" section in Methods).

The upper section is composed of the main channel and the lid bearing inlets/outlets. This section is assembled separately and mounted on the lower section before the experiment starts. The main channel (Y-shaped, 45×5 mm in size, inlets diameter 2.5 mm) is assembled by stacking three layers of PSA intercalated by two layers of polystyrene, reaching a total height of 500 µm. The lid is obtained by razor cutting three holes (2 inlets, 1 outlet) of 2.5 mm diameter into a low auto-fluorescence COP layer. All PSA, PS, and COP layers are exposed to 30 min UV light before assembly for sterilization purposes.

PAA hydrogel polymerization

To generate PAA gel with a stiffness gradient we adapted the slide-mask photopolymerization technique developed by Sunyer and co-workers[53]. A 2 µl drop of acrylamide mix (10% acrylamide, 0.5% bis-acrylamide; 740 µg/ml of Irgacure; a 1:25 dilution of saturated solution of (-)Riboflavin; and 1:250 dilution of of 0.5 µm fluorescent beads) is casted inside the rectangular holes of the plasma treated gel pod layer (Fig. 1E, first PSA layer) and applied to a silanized (3-(trimethoxysilyl) propyl methacrylate) glass slide (Fig. 1E, glass layer). The solution is covered with a glass coverslip made hydrophobic by treatment with Repel Silane. Gradients are generated by initially covering the acrylamide mix with an opaque mask and then slowly sliding it at a controlled speed while irradiating with a UV bench lamp of 365 nm (UVP) (Fig. 1C). The mask is slid using Labview-controlled (NI) piston of an automatic syringe pump machine (Harvard Apparatus 22). To ensure full polymerization, the mask is first slid at a speed of 400µm/s for 1s (uncovering an area for initial nucleation of the polymerization reaction), and then at 14.5 µm/s for 240s. After gel photopolymerization, the hydrophobic glass coverslip is removed and the gel is washed with ddH_2O thoroughly to remove unreacted reagents. Mechanical gradients are mapped using custom made AFM. Before cell seeding, gels are activated with 5 µl/gel of Sulfo-Sanpah (final concentration 2 mg/ml) and exposed to UV light for 3 min. The activated gels are finally coated with 100 µg/ml of Collagen I for 2 hours at room temperature, and subsequently washed thoroughly with PBS to remove excess.

Device characterization and validation

Chemical gradient

Chemical gradients are typically used to study directed cell migration in response to spatial patterns of chemokine concentration[48,57]. Because the molecular weight of chemokines typically ranges between 6 and 14 kDa (e.g. SDF1, CCL19, IL-8 etc) or even lower (cAMP, LTB4, fMLP)[58] we characterized

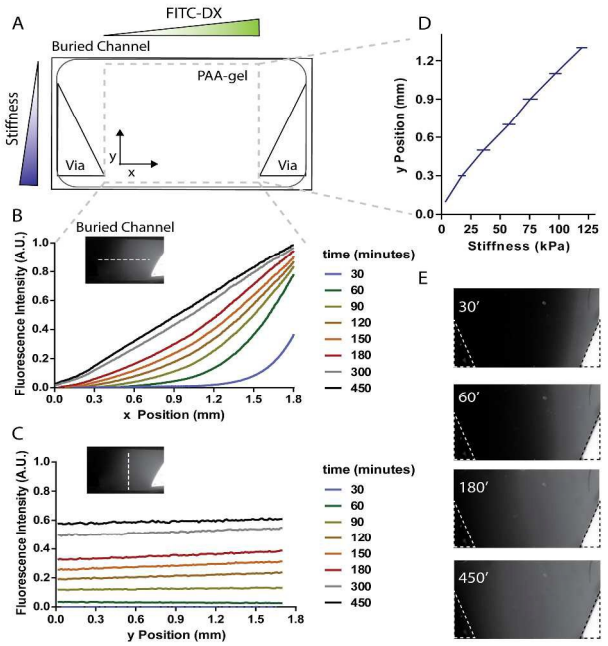

Fig 2 Characterization of chemical and mechanical gradients within the buried channel. (A) Scheme of a buried channel. A linear chemical gradient is generated between the vias of the buried channel (horizontal axis). A PAA-gel with a stiffness gradient is generated along the vertical axis of the buried channel. (B) The application of a dual flow (source solution = 100µg/ml 10kDa FITC-dx in HEPES buffer 10 mM; sink solution = HEPES buffer 10 mM) allows for the generation of a linear gradient in ~300 minutes. Fluorescence intensity profiles are computed every 30 minutes. Further quantification at 450 minutes is reported to show that the diffusive gradient is stable. Inset shows the dashed line across which intensity is measured. (C) Fluorescence intensity is homogeneous along the direction perpendicular to the FITC-dx gradient direction. (D) Stiffness profile measured by AFM along the vertical axis of the gel. Lowest measured stiffness is 1kPa, increasing with a gradient of ~80 kPa/mm, and reaching a maximum stiffness at ~120 kPa. (E) Representative snap shots show the diffusion of FITC-dx inside the buried channel. Dashed triangles indicate the vias.

gradient formation in our device using fluorescein isothiocyanate dextran 10kDa (FITC-dx 10kDa) as fluorescent reporter. We note that the device also creates a linear gradient with higher molecular weight although at a slower rate (Supplementary Fig. S3).

To establish the diffusive gradient we introduced through the device's inlets a sink solution (HEPES buffer, 10 mM) and a source solution (100 µg/ml of FITC-dx 10 kDa). Both solutions were flowed in parallel at 7 µl/min (Fig.1B). Given that the vias at both sides of the buried channel were exposed to the same pressure, a linear diffusive gradient was established along the horizontal axis of the buried channel (Fig. 2A). To monitor the evolution of the diffusive gradient we acquired time lapse images of the buried channel every 30 minutes using a 4× objective. The triangular vias layer (Fig. 1E) was made opaque with black ink before device assembly to avoid background fluorescence from the upper channel. Correction of the images was performed according to established protocols[56]. The quantification of the pixel intensity showed that a linear gradient was mainly formed by diffusion and reached a steady state after 300 minutes (Fig. 2B and 2E). Due to the large width of the buried channel (1.8 mm), we also checked the orthogonal fluorescence profile. As shown in Fig. 2C, fluorescent intensity was homogeneously distributed along the perpendicular direction of the buried channel.

Mechanical gradient

The stiffness gradients were characterized by measuring Young's modulus of the PAA gels using an Atomic Force Microscope (see "Methods and reagents" section below). The obtained gel stiffness profile was largely linear and spanned from 1 kPa to 120 kPa, a range that closely represent physiological of extracellular matrix stiffness[59]. In the design conditions described above, the stiffness gradient was 80 kPa/mm (Fig. 2D). By varying the concentrations of acrylamide or bis-acrylamide in the PAA gel mix and the speed of the mask, gradients from 10 kPa/mm to 100 kPa/mm can be obtained.

HGF scattering assay

To validate our experimental setup we used the MDCK scattering assay. In this assay, islands of epithelial cells dissociate and migrate away from each other as individual cells in response to HGF (also known as scatter factor). This model has extensively been studied because it captures key aspects of the epithelial to mesenchymal transition (EMT)[25]. In particular, previous work has established that the scattering of epithelial clusters depends on the concentration of HGF and on the stiffness of the substrate[15], thus making this assay an ideal candidate to test the performance of our microfluidic chip. To carry out the dynamic cell scattering assay, we used the microfluidic chip to deliver a gradient of HGF (source solution at 5 ng/ml) across a population of MDCK cells seeded onto a compliant substrate with orthogonal stiffness gradient ranging from 1 to 120 kPa. Thus depending on the cell position within the channel, MDCK cells were exposed to mutually independent levels of HGF concentration and substrate stiffness (Fig. 3A and 3B, Supplementary movie 1). Cells were imaged for 24-48h immediately after the application of the HGF gradient. To systematize the quantification of the assay, we segmented images of the buried channel in a 3 by 2 matrix: 3 rows defining regions of low (1-30 kPa), medium (30-70 kPa) and high (70-120 kPa) stiffness, and 2 columns defining regions of high and low HGF concentration (Fig. 3A, colored frames).

We first monitored the position and the speed of every cell in the buried channel. During the initial hours of the assay, MDCKs increased their velocity at a similar rate in all 6 regions of the chip (Fig. 3C). At ≈ 16h, cells in the low HGF region reached a plateau whose value was independent of the stiffness of the substrate. This result is in agreement with previous observations showing that kinematics of untreated MDCK cells are largely independent on the stiffness of the substrate[55]. By contrast, cells in high-HGF regions peaked at ≈ 25h with peak values increasing

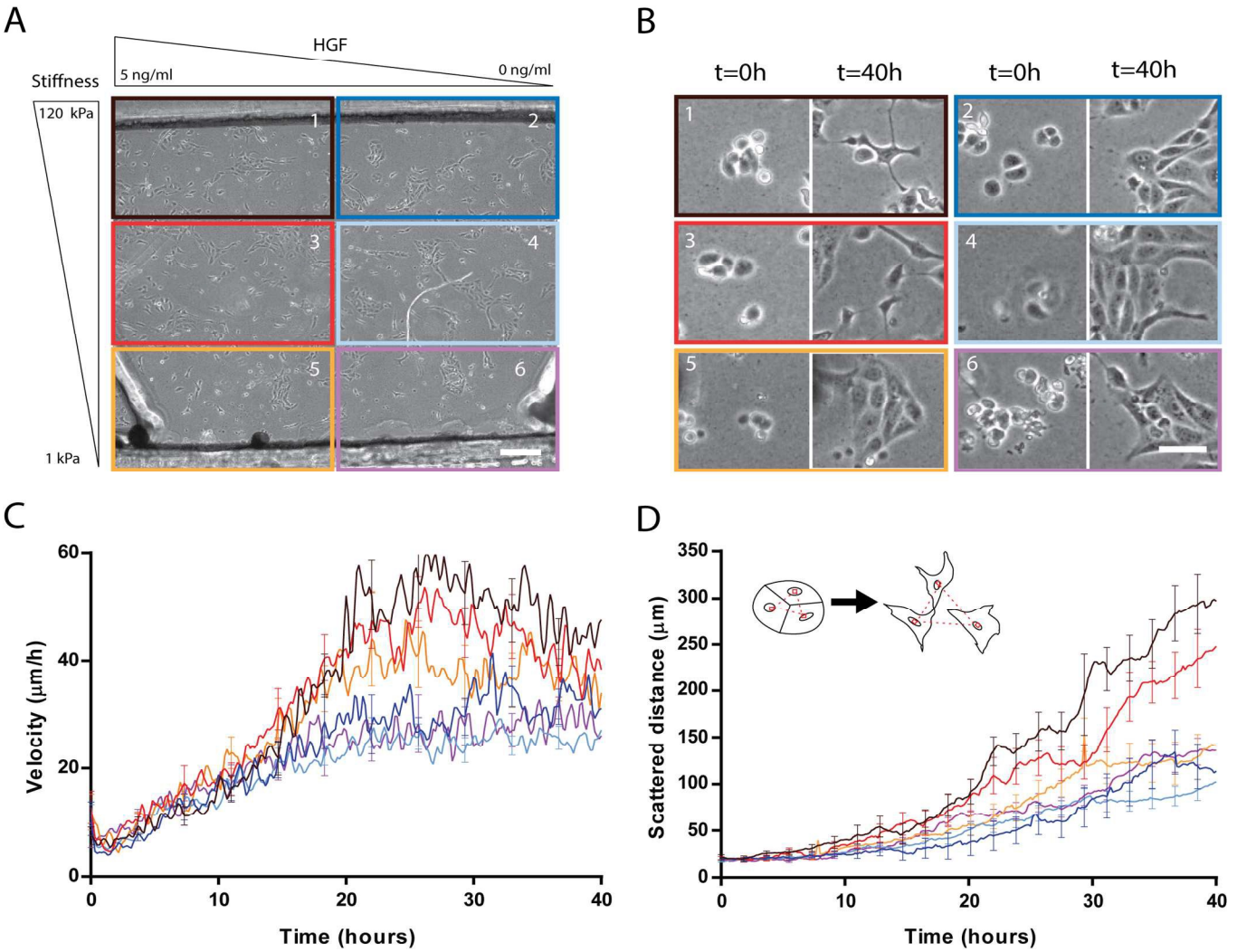

Fig 3. Device validation using HGF scattering assay. (A) Cells inside the buried channel are exposed to an HGF concentration gradient of 2.8 ng/(ml·mm) ranging from 0 to 5 ng/ml and a stiffness gradient of 80 kPa/mm ranging from 1 to 120 kPa. To systematize the analysis, the field of view is divided in a 3 by 2 matrix in which data are averaged (high-mid-low stiffness and high-low HGF concentration), scale bar = 200 µm. (B) Representative images of the cells in each region of the 3 by 2 matrix, scale bar = 50 µm. (C) Time evolution of cell velocity for each of the 6 regions (same color coding than A). (D) Time evolution of the scattered distance for each of the 6 regions (same color coding than A).

with substrate stiffness. This result is in agreement with previous observations showing that the kinematic response to HGF depends on substrate stiffness[15]. To further validate our assay, we analyzed the scattering dynamics in the 6 regions of the chip (Fig. 3B and 3D). Visual inspection of each region showed that cell clusters located on the high-HGF/high-stiffness region scattered readily, whereas those located in the low-HGF/low-stiffness remained cohesive and proliferated (Fig. 3B). To quantify scattering dynamics, we computed the time evolution of the average distance of the cells that at t = 0h were clustered (Fig. 3C, inset). Scattering dynamics increased with time for all conditions (Fig. 3D) but at different rates and to a different extent. As expected, no significant differences in scattering were observed in cells seeded at low HGF concentration. By contrast, the scattered distance increased significantly with substrate stiffness in regions subjected to high HGF.

Interestingly, in regions of high HGF but low stiffness (Fig. 3D, orange curve), the scattered distance was comparable with the low HGF regions. This set of experiments shows that cell scattering is a phenomenon synergistically regulated by EMT inducing scatter factor and substrate stiffness, and that these synergistic conditions are effectively created inside the test chamber of our microfluidic device.

Traction Force Microscopy

To demonstrate that traction force measurements can be performed in our microfluidic chip, we added 0.5 µm fluorescent beads (Invitrogen) to the PAA gels. After cell attachment and for each time frame, we obtained an image of the fluorescent beads

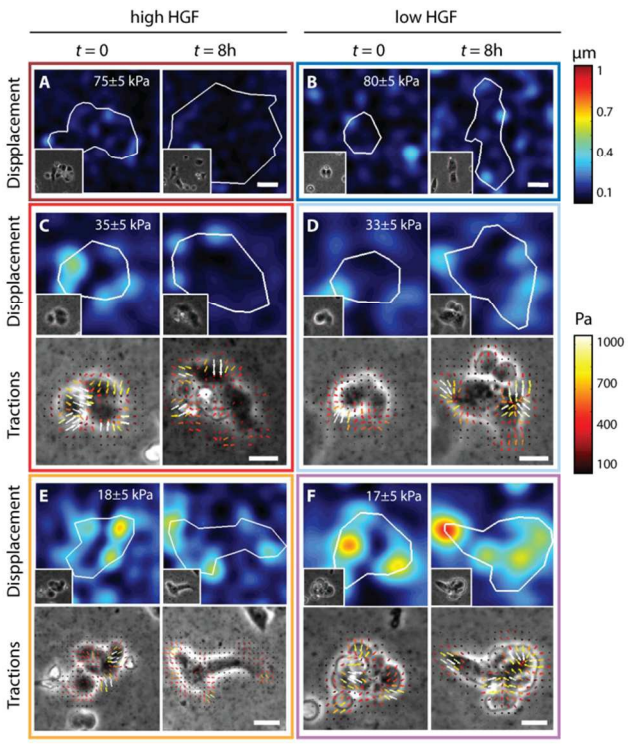

Fig 4. Displacement (top) and traction (bottom) force fields of representative clusters during the long-term microfluidic experiment. Maps are shown at $t = 0$ (before HGF gradient establishment) and $t \approx 8$h. Color coding of each panel corresponds to that in Fig. 3. For the highest stiffness (A,B), displacement fields were below optical resolution and traction fields could not be estimated.

at the top surface of the gel (stressed gel image). At the end of the experiment, cells were detached with trypsin and we obtained an image of the relaxed gel (unstressed gel image). Using both images (stressed and unstressed gel images), we computed the displacement of the gel surface caused by the cells using a custom built particle imaging velocimetry (PIV) software. Because gel stiffness varies in space, traction forces cannot be recovered from the displacements of the gel surface using traditional traction force cytometry. To overcome this limitation to a first order approximation, we assumed that the value of Young's modulus was constant across the area of each cell cluster. For each cluster, this value of the local Young's modulus was obtained from the AFM calibration. We then used Fourier Transform Traction force microscopy[54] to estimate traction forces. Fig. 4 shows representative displacement and traction force fields for cells located in the different regions of the microfluidic chip before (t=0h) and after (t=8h) HGF stimulation. In the highest stiffness regions (>70 kPa), the displacements of the PAA gels were below the optical resolution and tractions could not be computed (Fig. 4A and 4B). In substrate regions of lower stiffness we observed appreciable gel deformations (~1 μm), from which we computed traction maps (Fig. 4C-F). As commonly observed in MDCK clusters, tractions were restricted to the cluster periphery with an average value on the order of 0.5 kPa[60]. These experiments show that our setup enables the measurement of exact substrate displacements across the range of physiological stiffness and that traction maps can be estimated from these displacements.

Discussion and conclusions

We described a simple microfluidic device built with low cost non-elastomeric components and machinery, which is designed to investigate cellular responses to independent chemical and mechanical cues varying across space. The combination of chemical and mechanical cues in a microfluidic chip have been previously demonstrated through the generation of gradients of chemical concentration and shear stress[61–63]. Here we reported a device that generates a stable, linear and diffusive chemical gradient over a cell population cultured on a PAA hydrogel with a linear stiffness gradient perpendicular to the chemical gradient. Using MDCK cells as a model, we validated the device by analyzing the relation between the scattering factor HGF and the stiffness of the underlying extracellular matrix. Consistent with current literature, we observed that MDCK scattering depended on the synergy between HGF concentration and substrate stiffness. Moreover, the device also allowed traction force measurements of MDCK clusters.

Although our device offers great control over the two physiological stimuli, it has a few limitations. For example chemical gradients are established by passive diffusion, which is a slower method than convection-based gradient generators[21], and it does not offer control over gradient shape. Despite these limitations, our device tackles unsolved issues such as how to introduce two stimuli of different nature (concentration and stiffness) in a controlled fashion, and how to fabricate such a controlled micro-environment with accessible materials and equipment. In principle, our approach could be generalized to the production of orthogonal chemical and mechanical gradients in 3D conditions by filling the buried channels with 3D hydrogels with stiffness gradients.

In general, cells show distinct responses to the local value of an environmental cue (chemical concentration or substrate stiffness in our case)[64] and to its spatial gradient[10,65]. To validate the device unambiguously, it was thus important to choose a well-characterized model system in which cells responded either to the magnitude of the cue or to its spatial gradient, but not to both. We chose epithelial scattering of the MDCK cells as a model. In this model, cells respond to the concentration of HGF and to the stiffness of the substrate, but not their respective gradients (Supplementary Fig. S2). Although our validation was not aimed at analyzing migratory responses to gradients, our device is perfectly suited to study the synergy or competition between chemotaxis and durotaxis.

In addition, we expect our microfluidic cell assay to prove useful in high throughput assays in which many chemical and mechanical conditions need to be tested. One example is drug discovery in cancer preclinical trials in which the synergies between chemical and mechanical cues have been too difficult to address[66]. Because our device needs small amounts of cells, these

drug screening assays could also use primary cells, which display a more physiological phenotype than cell lines, but are costly to use in large quantities. Our microfluidic chip is also widely applicable to mechanobiology, developmental biology and cancer. Indeed, in the past 15 years, mechanical cues have been added to chemical factors as potent regulators of cellular processes but cross-talk between chemical and mechanical cues remains poorly understood, in part because it requires tedious experiments with multiple well plates using single stiffness matrices and manual dilutions. We believe that our microfluidic device provides a robust and well-defined cell micro-environment to interrogate the interplay between chemistry and mechanics in a single chip.

Methods and reagents

Reagent and cell culture

Gel mix was prepared using the following reagents: 40% acrylamide (BioRad, 161-0140); 2% bis-acrylamide (BioRad, 161-0142); Irgacure 2959 (BASF); (-) Riboflavin (Sigma-Aldrich) and 0.5 µm fluorescent beads (Life Technologies). Gels were activated with Sulfo-SANPAH (4822589, Cultek) and coated with rat tail Collagen I (ThermoScientific). Glass slides were activated using a solution containing 3-(trimethoxysilyl) propyl methacrylate, (Sigma-Aldrich):etanol:acetic acid:ddH20 (5:200:1800:8000). Glass coverslips were passivated using Repel Silane (GE). For characterization purposes Fluorescein-dextran 10kDa (FD10S, Sigma-Aldrich) was used. Scattering assay was performed using a dilution of reconstituted rhHGF (100-39, Peprotech). MDCK strain II cells (ATCC) were cultured in minimum essential media with Earle's Salts and l-glutamine (Gibco) supplemented with 10% fetal bovine serum (FBS; Gibco), 100 U/ml penicillin and 100 µg/ml streptomycin (complete medium).

Cell loading

MDCK-II cells were seeded at a concentration of 10^6 cells/ml before the assembly of the upper and lower sections of the system. After allowing cells to adhere to the PAA hydrogel in a standard incubator with temperature and CO2 control, the upper section was mounted and the system was connected through magnetic connectors[67] to appropriate tubing. After 4 hours at 37ºC and 5% CO2 cells were adherent to the PAA hydrogel at a uniform density (Fig 3A, Supplementary video 1).

Atomic Force Microscopy measurements

For Atomic Force Microscopy measurements, we used a custom-built AFM attached to an inverted optical microscope (Ti-Eclipse, Nikon) as described previously[68]. Gels were indented with a V-shaped cantilever (Bruker) with a triangular tip and a nominal spring constant calibrated by the thermal fluctuations method[69,70].

Given the wide stiffness range of the gels, we used a nominal spring constant of k = 0.03 N/m to ensure that for all measurements cantilever deflection was within the linear detection range of the AFM. The relationship between the photodiode signal and the cantilever deflection was computed from the slope of the force displacement curve obtained at a bare region of the coverslip (without gel sample). For each sample, we acquired 5 force-displacement (F-z) curves (where $F = kd$, d being the deflection and z being piezotranslator position) by ramping forward and backward the cantilever at a constant speed (5 µm amplitude, 1 Hz and ~1µm of indentation). Each experimental F-z curve was fitted to the four-sided pyramidal indenter model[71]:

$$F = \frac{3\,E\,\tan\theta}{4(1-\nu^2)}\delta^2$$

where E is the Young's modulus, ν is the Poisson's ratio, θ is de semi-included angle of the pyramidal indenter, and δ is the indentation depth. The parameter ν is assumed to be 0.5 (the water-filled hydrogel essentially is incompressible), and the indentation depth is calculated as $\delta = z - z_0 - d$, where z_0 is the tip-gel contact point. E and z_0 were estimated by least-squares fit of this equation to the F-z curve recorded on each gel point. We measured the Young's modulus of the gel every 200 µm along the axis of maximum gel stiffness change. Measurements were taken in n = 5 different gels.

Microscopy

Time lapse movies were obtained by imaging the buried channels every 10 minutes using a motorized Ti-Eclipse microscope (Nikon) and a 10× objective. Several adjacent images were obtained to cover all area of the buried channel. Images were stitched using a custom made Matlab script (The Mathworks). Cells in each sector of the buried channel were manually tracked using Manual Tracker imageJ plugin, allowing for evaluation of average cell position and speed

Acknowledgements

This work was funded by the Spanish Ministry of Economy and Competitiveness (BFU2012-38146), the Generalitat de Catalunya (2014-SGR-927), the European Research Council (StG-242993 and CoG-616480), and the U.S. National Institute of Standards and Technology (70NANB14H271). The authors wish to thank Lluis Mulero from Digital-graphic (Barcelona) for material support during the early phase of the project, Dr. Mateu Pla-Roca (Platform of Nanotechnology, IBEC) for his help with early trial assemblies using hot embossing, Prof. Antoni Homs for COP supplies, Michael O'Brien from Adhesives Research for supplying PSA samples, and Daniela Missori for her suggestions on device design.

Notes and references

1 K. S. Zaret, *Cell Stem Cell*, 2009, 4, 373–374.
2 S. Chetty, F. W. Pagliuca, C. Honore, A. Kweudjeu, A. Rezania and D. a Melton, *Nat. Methods*, 2013, **10**, 553–6.
3 A. Aderem and R. J. Ulevitch, *Nature*, 2000, **406**, 782–787.
4 S. Koyama, K. J. Ishii, C. Coban and S. Akira, *Cytokine*, 2008, 43, 336–341.
5 P. V. Afonso, M. Janka-Junttila, Y. J. Lee, C. P. McCann, C. M. Oliver, K. A. Aamer, W. Losert, M. T. Cicerone and C. A. Parent, *Dev. Cell*, 2012, **22**, 1079–1091.
6 C. J. Drake, A. LaRue, N. Ferrara and C. D. Little, *Dev. Biol.*, 2000, **224**, 178–188.
7 J. R. Conejo-Garcia, F. Benencia, M.-C. Courreges, E. Kang, A. Mohamed-Hadley, R. J. Buckanovich, D. O. Holtz, A. Jenkins, H. Na, L. Zhang, D. S. Wagner, D. Katsaros, R. Caroll and G. Coukos, *Nat. Med.*, 2004, **10**, 950–958.
8 A. J. Engler, S. Sen, H. L. Sweeney and D. E. Discher, *Cell*, 2006, **126**, 677–89.
9 O. Chaudhuri and D. J. Mooney, *Nat. Mater.*, 2012, 11, 568–569.
10 C. M. Lo, H. B. Wang, M. Dembo and Y. L. Wang, *Biophys. J.*, 2000, **79**, 144–152.
11 D. T. Tambe, C. C. Hardin, T. E. Angelini, K. Rajendran, C. Y. Park, X. Serra-Picamal, E. H. Zhou, M. H. Zaman, J. P. Butler, D. A. Weitz, J. J. Fredberg and X. Trepat, *Nat. Mater.*, 2011, **10**, 469–475.
12 T. Mammoto and D. E. Ingber, *Development*, 2010, **137**, 1407–20.
13 V. Swaminathan, K. Mythreye, E. Tim O'Brien, A. Berchuck, G. C. Blobe and R. Superfine, *Cancer Res.*, 2011, **71**, 5075–5080.
14 M. Puig, R. Lugo, M. Gabasa, A. Gimenez, A. Velasquez, R. Galgoczy, J. Ramirez, A. Gomez-Caro, O. Busnadiego, F. Rodriguez-Pascual, P. Gascon, N. Reguart and J. Alcaraz, *Mol. Cancer Res.*, 2014, 8–10.
15 J. De Rooij, A. Kerstens, G. Danuser, M. A. Schwartz and C. M. Waterman-Storer, *J. Cell Biol.*, 2005, **171**, 153–164.
16 M. J. Paszek, N. Zahir, K. R. Johnson, J. N. Lakins, G. I. Rozenberg, A. Gefen, C. A. Reinhart-King, S. S. Margulies, M. Dembo, D. Boettiger, D. A. Hammer and V. M. Weaver, *Cancer Cell*, 2005, **8**, 241–254.
17 J. Alcaraz, R. Xu, H. Mori, C. M. Nelson, R. Mroue, V. A. Spencer, D. Brownfield, D. C. Radisky, C. Bustamante and M. J. Bissell, *EMBO J.*, 2008, **27**, 2829–2838.
18 J. L. Leight, M. A. Wozniak, S. Chen, M. L. Lynch and C. S. Chen, *Mol. Biol. Cell*, 2012, 23, 781–791.
19 A. Marinkovic, J. D. Mih, J.-A. Park, F. Liu and D. J. Tschumperlin, *AJP Lung Cell. Mol. Physiol.*, 2012, 303, L169–L180.
20 F. Liu, J. D. Mih, B. S. Shea, A. T. Kho, A. S. Sharif, A. M. Tager and D. J. Tschumperlin, *J. Cell Biol.*, 2010, **190**, 693–706.
21 M. C. Markowski, A. C. Brown and T. H. Barker, *J. Biomed. Mater. Res. - Part A*, 2012, **100 A**, 2119–2127.
22 J. M. Lee, S. Dedhar, R. Kalluri and E. W. Thompson, *J. Cell Biol.*, 2006, **172**, 973–981.
23 J. P. Thiery, H. Acloque, R. Y. J. Huang and M. A. Nieto, *Cell*, 2009, 139, 871–890.
24 I. Royal, N. Lamarche-Vane, L. Lamorte, K. Kaibuchi and M. Park, *Mol. Biol. Cell*, 2000, **11**, 1709–25.
25 V. Maruthamuthu and M. L. Gardel, *Biophys. J.*, 2014, **107**, 555–563.
26 D. Irimia, *Annu. Rev. Biomed. Eng.*, 2010, **12**, 259–284.
27 J. Wu, X. Wu and F. Lin, *Lab Chip*, 2013, **13**, 2484–99.
28 E. K. Sackmann, A. L. Fulton and D. J. Beebe, *Nature*, 2014, **507**, 181–9.
29 L. S. Kim SH, Lee GH, Park JY, *J. Lab. Autom.*, 2015, **20**, 82–95.
30 A. G. G. Toh, Z. P. Wang, C. Yang and N.-T. Nguyen, *Microfluid. Nanofluidics*, 2013, **16**, 1–18.
31 G. Gerisch and H. U. Keller, *J. Cell Sci.*, 1981, **52**, 1–10.
32 C. A. Parent, B. J. Blacklock, W. M. Froehlich, D. B. Murphy and P. N. Devreotes, *Cell*, 1998, **95**, 81–91.
33 E. Theveneau, L. Marchant, S. Kuriyama, M. Gull, B. Moepps, M. Parsons and R. Mayor, *Dev. Cell*, 2010, **19**, 39–53.
34 X. Zhao, S. Jain, H. B. Larman, S. Gonzalez and D. J. Irvine, *Biomaterials*, 2005, **26**, 5048–5063.
35 B. J. Kim and M. Wu, *Ann. Biomed. Eng.*, 2012, 40, 1316–1327.
36 D. Irimia, D. A. Geba and M. Toner, *Anal. Chem.*, 2006, **78**, 3472–3477.
37 G. Velve-Casquillas, M. Le Berre, M. Piel and P. T. Tran, *Nano Today*, 2010, **5**, 28–47.
38 N. Li Jeon, H. Baskaran, S. K. W. Dertinger, G. M. Whitesides, L. Van de Water and M. Toner, *Nat. Biotechnol.*, 2002, **20**, 826–830.
39 G. M. Walker, H. C. Zeringue and D. J. Beebe, *Lab Chip*, 2004, **4**, 91–97.
40 V. V Abhyankar, M. A. Lokuta, A. Huttenlocher and D. J. Beebe, *Lab Chip*, 2006, **6**, 389–393.
41 H. Wu, B. Huang and R. N. Zare, *J. Am. Chem. Soc.*, 2006, **128**, 4194–4195.
42 W. Saadi, S. W. Rhee, F. Lin, B. Vahidi, B. G. Chung and N. L. Jeon, *Biomed. Microdevices*, 2007, **9**, 627–635.
43 H. Xu and S. C. Heilshorn, *Small*, 2013, **9**, 585–595.
44 A. Shamloo, M. Manchandia, M. Ferreira, M. Mani, C. Nguyen, T. Jahn, K. Weinberg and S. Heilshorn, *Integr. Biol.*, 2013, **5**, 1076–1085.
45 C. Zhang, S. Jang, O. C. Amadi, K. Shimizu, R. T. Lee and R. N. Mitchell, *Biomed Res. Int.*, 2013, **2013**.
46 H. Xu, M. M. Ferreira and S. C. Heilshorn, *Lab Chip*, 2014, **14**, 2047–56.
47 H. V Prentice-Mott, C.-H. Chang, L. Mahadevan, T. J. Mitchison, D. Irimia and J. V Shah, *Proc. Natl. Acad. Sci. U. S. A.*, 2013, **110**, 21006–11.
48 L. Boneschansker, J. Yan, E. Wong, D. M. Briscoe and D. Irimia, *Nat. Commun.*, 2014, **5**, 4787.
49 Y. Zhou and Q. Lin, *Sensors Actuators B Chem.*, 2014, **190**, 334–341.
50 M. Raab, J. Swift, P. C. D. P. Dingal, P. Shah, J.-W. Shin and D. E. Discher, *J. Cell Biol.*, 2012, **199**, 669–83.
51 J. Y. Wong, A. Velasco, P. Rajagopalan and Q. Pham, *Langmuir*, 2003, **19**, 1908–1913.
52 N. Zaari, P. Rajagopalan, S. K. Kim, A. J. Engler and J. Y. Wong, *Adv. Mater.*, 2004, **16**, 2133–2137.
53 R. Sunyer, A. J. Jin, R. Nossal and D. L. Sackett, *PLoS One*, 2012, **7**.
54 J. P. Butler, I. M. Tolić-Nørrelykke, B. Fabry and J. J. Fredberg, *Am. J. Physiol. Cell Physiol.*, 2002, **282**, C595–C605.
55 X. Trepat, M. R. Wasserman, T. E. Angelini, E. Millet, D. A. Weitz, J. P. Butler and J. J. Fredberg, *Nat. Phys.*, 2009, 5, 426–430.
56 J. Atencia, G. A. Cooksey and L. E. Locascio, *Lab Chip*, 2012, 12, 309.

57 H. Cho, T. Hashimoto, E. Wong, Y. Hori, L. B. Wood, L. Zhao, K. M. Haigis, B. T. Hyman and D. Irimia, *Sci. Rep.*, 2013, **3**, 1823.

58 E. J. Fernandez and E. Lolis, *Annu. Rev. Pharmacol. Toxicol.*, 2002, **42**, 469–499.

59 I. Levental, P. C. Georges and P. A. Janmey, *Soft Matter*, 2007, 3, 299.

60 A. F. Mertz, S. Banerjee, Y. Che, G. K. German, Y. Xu, C. Hyland, M. C. Marchetti, V. Horsley and E. R. Dufresne, *Phys. Rev. Lett.*, 2012, **108**.

61 J. Y. Park, S. J. Yoo, C. M. Hwang and S.-H. Lee, *Lab Chip*, 2009, **9**, 2194–2202.

62 J. Y. Park, S. Takayama and S.-H. Lee, *Integr. Biol. (Camb).*, 2010, **2**, 229–240.

63 H. W. Wu, C. C. Lin, S. M. Hwang, Y. J. Chang and G. B. Lee, *Microfluid. Nanofluidics*, 2011, **11**, 545–556.

64 A. J. Engler, S. Sen, H. L. Sweeney and D. E. Discher, *Cell*, 2006, **126**, 677–689.

65 R. A. Jannat, M. Dembo and D. A. Hammer, *Biophys. J.*, 2011, **101**, 575–584.

66 N. E. Sounni and A. Noel, *Clin. Chem.*, 2013, **59**, 85–93.

67 J. Atencia, G. A. Cooksey, A. Jahn, J. M. Zook, W. N. Vreeland and L. E. Locascio, *Lab Chip*, 2010, **10**, 246–249.

68 J. Alcaraz, L. Buscemi, M. Grabulosa, X. Trepat, B. Fabry, R. Farré and D. Navajas, *Biophys. J.*, 2003, **84**, 2071–2079.

69 J. L. Hutter and J. Bechhoefer, *Rev. Sci. Instrum.*, 1993, **64**, 1868–1873.

70 H. J. Butt and M. Jaschke, *Nanotechnology*, 1995, **6**, 1–7.

71 F. Rico, P. Roca-Cusachs, N. Gavara, R. Farré, M. Rotger and D. Navajas, *Phys. Rev. E - Stat. Nonlinear, Soft Matter Phys.*, 2005, **72**.